

The Magnetic Field Produced from a Conical Current Sheet and from a Thin and Tightly-Wound Conical Coil

Matthew Smith¹, Nikiforos Fokas¹, Kevin Hart²,
Slobodan Babic³, and Jerry P. Selvaggi^{1, *}

Abstract—Mathematical expressions for the components of the magnetic field produced by a conically-shaped current sheet and by a tightly-wound conical coil are presented. The conical current sheet forms the frustum of a cone. In the limit as the top radius of the frustum approaches the bottom radius, a cylindrical current sheet is formed. Mathematical expressions for the magnetic field produced by a cylindrical current sheet are then compared to known and published results.

1. INTRODUCTION

Analytical expressions for the off-axis components of magnetic field produced from a conical current sheet do not appear to be forthcoming in the literature. However, semi-analytical expressions as well as purely numerical results do exist. This article presents a method for analytically evaluating the magnetic field produced from a conical current sheet. The components of the magnetic field are then compared to the components of the magnetic field produced by an infinitely-thin and tightly-wound conical coil. The lead wires for the coil and for the current sheet are not considered since the contribution to the magnetic field from these sources can always be taken into account by employing linear superposition.

Before proceeding with any analysis, one should consider the limitations of any proposed model. To this end, the fine structure contribution of the magnetic field [1] due to the helical nature of the conical coil [2], as well as its geometric cross section, is not considered. Therefore, the effect of the axial component of current, which must exist for any conical coil with a nonzero pitch, is ignored. The same can be said about the fine structure contribution of the magnetic field due to a conical current sheet. The thickness of conical sheet is being ignored, and therefore the computed magnetic field at observation points very close to the current sheet should be viewed with skepticism.

Due to these restrictions, one should use caution when computing the magnetic field at observation points very close to the current source. One can most certainly employ all the equations developed in Section 2 to compute the magnetic field at any point in space not coincident with the source, but for those observation points close to the source, the computed magnetic field may not yield a true representation of the measured magnetic field from a real conical coil or from a real conical current sheet. However, for observation points that are not “too close” to the current source, and for which any first-order effects are negligible, the equations for the magnetic field in Section 2 should work well.

In this context, any first-order effect is one in which the thickness of the sheet, the cross-section of the coil, and the pitch of the coil would be enough to perturb the field in such a way as to negate the effectiveness of the proposed mathematical model for observation or field points close to the current source. The more closely the design of the conical current sheet or the conical coil comes to its theoretical

Received 18 September 2020, Accepted 16 December 2020, Scheduled 26 December 2020

* Corresponding author: Jerry P. Selvaggi (jpsst44@gmail.com).

¹ Division of Engineering Programs at SUNY New Paltz, 1 Hawk Dr., New Paltz, New York, NY 12561, USA. ² Knolls Atomic Power Lab in Schenectady, New York, USA. ³ Departments of Physics and Electrical Engineering at Ecole Polytechnique de Montreal, QC, Canada.

model, the more confidence one should have in the computation of the magnetic field near the magnetic source.

The approximation of a thin current sheet and an infinitely-thin and tightly-wound coil seems, at first, to be rather a restrictive condition. However, for those practical applications which involve a desire to know the magnetic field at points off the symmetry axis but not “too close” to the current source, the mathematical expressions developed in this article can be employed for both numerical and analytical purposes.

The current in both the conical current sheet and conical coil is assumed to flow in a strictly azimuthal direction. The starting point will be to develop the magnetic vector potential [3, 4] and then to introduce a number of equivalent expressions for the components of the magnetic field. A series of numerical examples are explored in order to test the accuracy of the analytical expressions. All mathematical expressions have been checked using Mathematica [5]. This is done in order to develop a common base line so that anyone reading this article can more easily reproduce all the mathematical and numerical results. Also, the authors felt that Mathematica [5] has all the necessary analytical tools to more easily develop the analytical expressions. This becomes important when finding the magnetic field at points off the symmetry axis where the mathematics invariably becomes more complex.

2. CONICAL CURRENT SHEET AND CONICAL COILS

2.1. Conical Current Sheet Model

An ideal geometric model chosen for a thin and conically-shaped current sheet is represented by the frustum of a cone as illustrated in Fig. 1 [6]. The authors will present a number of equivalent expressions for computing the magnetic field from a conical current sheet. All bold-faced quantities are defined to be vector quantities.

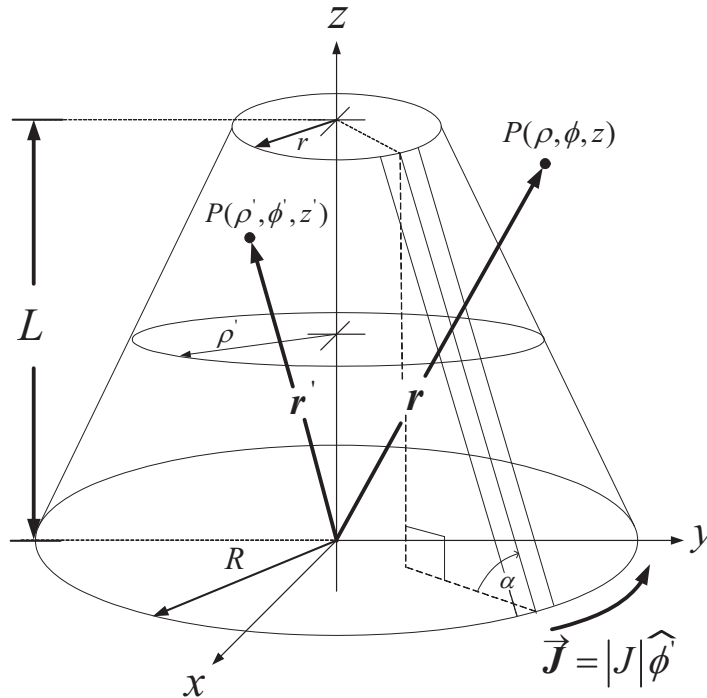


Figure 1. Conical current sheet.

Assume that the current sheet exhibits only an azimuthally-directed current density as shown in Fig. 1.

$$\mathbf{J} = J\hat{\phi}, \quad (1)$$

where $\hat{\phi}'$ is the unit vector in the azimuthal direction, and $J = |\mathbf{J}|$ has units of *Amperes*(A) per unit length. From Fig. 1, define the parameter, κ , as

$$\kappa = \frac{R - r}{L}, \quad (2)$$

where $\kappa = \cot(\alpha)$. The authors assume that J is a constant. However, this is not a mandatory condition for the following analysis to be effectively applied. Also, as $\kappa \rightarrow 0$ or $r \rightarrow R$, the thin and hollow frustum degenerates to a thin and hollow cylinder. The cylindrical current sheet is considered in Section 4, and the analysis illustrated in this section is a result of the limiting case of the conical current sheet.

All primed variables are defined as source variables, and all the unprimed variables are defined as the field or observation variables. The magnetic vector potential produced by the conical current sheet of Fig. 1 is

$$\mathbf{A} = \frac{\mu_0 J}{4\pi} \int_0^L \int_0^{2\pi} \frac{\rho'}{|\mathbf{r} - \mathbf{r}'|} \hat{\phi}' d\phi' dz', \quad (3)$$

where the azimuthal unit vector $\hat{\phi}' = -\sin(\phi')\hat{x} + \cos(\phi')\hat{y}$. In circular cylindrical coordinates, the distance between the field point and the source point is written as

$$|\mathbf{r} - \mathbf{r}'| = \sqrt{\rho^2 + \rho'^2 + (z - z')^2 - 2\rho\rho' \cos(\phi - \phi')}, \quad (4)$$

where ρ' is a function of z' given by

$$\rho' = R - \kappa z'. \quad (5)$$

Also, the authors define J to

$$J = N_t I_0, \quad (6)$$

where N_t is defined as the number of turns per unit length of the equivalent tightly-wound conical coil, and I_0 is a uniform current in *Amperes*. Choosing Eq. (6) as the defining magnitude of the current density allows for a simpler comparison between the magnetic field produced by a conical current sheet and that of a tightly-wound conical coil presented in Section 2.1. A similar idea can be found in Flax et al. [7]. This approach should become more clear as we proceed.

However, one may wish to define an alternative current density without introducing an equivalent turns per unit length, N_t . If this is the case then all subsequent analysis is still valid since we have assumed that J is a constant. For example, if one were to replace $N_t I_0$ in all subsequent equations with $J = I_0 / \sqrt{(R - r)^2 + L^2}$, which is exactly what the current density would be for an ideal current sheet, then the analysis remains unchanged. The goal is to find the magnetic field produced by a conical current sheet and compare it to the magnetic field produced by a tightly-wound conical coil.

The inverse distance function, $|\mathbf{r} - \mathbf{r}'|^{-1}$, given by Eq. (3) can be expanded in terms of toroidal harmonics [8–20] as follows:

$$\frac{1}{|\mathbf{r} - \mathbf{r}'|} = \frac{1}{\pi\sqrt{\rho\rho'}} \sum_{m=0}^{\infty} \varepsilon_m Q_{m-\frac{1}{2}}(\xi) \cos[m(\phi - \phi')], \quad (7)$$

where ε_m is 1 for $m = 0$; ε_m is 2 for all $m \geq 1$; and $\xi = \frac{\rho^2 + \rho'^2 + (z - z')^2}{2\rho\rho'} > 1$. The function $Q_{m-\frac{1}{2}}(\xi)$ is called the zeroth order Legendre function of half integral degree or toroidal function of zeroth order. Only the $m = 1$ term survives the azimuthal integration in subsequent analysis, and therefore only $Q_{\frac{1}{2}}(\xi)$ is needed for the azimuthally-directed vector potential. The $Q_{\frac{1}{2}}(\xi)$ term is then rewritten as a infinite series [15], and then employed for analytically evaluating the components of the magnetic field.

2.1.1. Magnetic Flux Density in Integral Form

Mathematical expressions written in integral form often form the basis of asymptotic analysis. For this reason, expressing the magnetic flux density in integral form may be quite useful. Also, when integrals are difficult to evaluate analytically, or their corresponding analytical expressions become cumbersome,

which is often the case when finding the magnetic field at observation points which lie off the symmetry axis, one may always resort to numerical integration in order to get accurate results. Introducing a few equivalent expressions for the magnetic flux density in integral form gives the reader some choices depending on the application.

For an azimuthally-directed current, the general expression for magnetic vector potential [3, 4] in Cartesian coordinates has only an x and a y component given by

$$A_x = -\frac{\mu_0 N_t I_0}{4\pi} \int_0^L \int_0^{2\pi} \frac{\rho' \sin(\phi')}{|\mathbf{r} - \mathbf{r}'|} d\phi' dz', \quad (8)$$

$$A_y = \frac{\mu_0 N_t I_0}{4\pi} \int_0^L \int_0^{2\pi} \frac{\rho' \cos(\phi')}{|\mathbf{r} - \mathbf{r}'|} d\phi' dz'. \quad (9)$$

Employing Eqs. (8) and (9) yield the general expressions for the components of the magnetic flux density in Cartesian and circular cylindrical coordinates as follows:

$$B_x = \frac{\mu_0 N_t I_0}{4\pi} \int_0^L \int_0^{2\pi} \frac{\rho'(z - z') \cos(\phi')}{|\mathbf{r} - \mathbf{r}'|^3} d\phi' dz', \quad (10)$$

$$B_y = \frac{\mu_0 N_t I_0}{4\pi} \int_0^L \int_0^{2\pi} \frac{\rho'(z - z') \sin(\phi')}{|\mathbf{r} - \mathbf{r}'|^3} d\phi' dz', \quad (11)$$

$$B_z = \frac{\mu_0 N_t I_0}{4\pi} \int_0^L \int_0^{2\pi} \frac{\rho' [\rho' - \rho \cos(\phi - \phi')]}{|\mathbf{r} - \mathbf{r}'|^3} d\phi' dz', \quad (12)$$

$$B_\rho = B_x \cos(\phi) + B_y \sin(\phi). \quad (13)$$

Now, substituting Eq. (7) in both Eq. (8) and Eq. (9) yields azimuthal component for the vector potential in cylindrical coordinates written as

$$\begin{aligned} A_\phi &= \frac{\mu_0 N_t I_0 \rho}{4} \sum_{n=0}^{\infty} \frac{(4n+1)!!}{(n+1)!n!} \left(\frac{\rho}{2}\right)^{2n} \int_0^L \frac{\rho'^{2n+2}}{[(\rho^2 + \rho'^2 + (z-z')^2)^{2n+\frac{3}{2}}]} dz', \\ &= \frac{\mu_0 N_t I_0}{8\sqrt{2}\rho} \int_0^L \frac{\sqrt{\rho'}}{\xi^{\frac{3}{2}}} F\left(\frac{3}{4}, \frac{5}{4}, 2, \frac{1}{\xi^2}\right) dz', \end{aligned} \quad (14)$$

where $F(\cdot)$ is the *Gauss hypergeometric function* [21, 22] expressed in Mathematica [5] as *Hypergeometric2F1*. From Eq. (14), the components of the magnetic flux density in circular cylindrical coordinates are

$$\begin{aligned} B_\rho &= -\frac{\partial A_\phi}{\partial z}, \\ &= \frac{3\mu_0 N_t I_0}{16\sqrt{2}\rho^{\frac{3}{2}}} \int_0^L \frac{(z-z')}{\xi^{\frac{5}{2}}\sqrt{\rho'}} \left\{ F\left(\frac{3}{4}, \frac{5}{4}, 2, \frac{1}{\xi^2}\right) + \frac{5}{8\xi^2} F\left(\frac{7}{4}, \frac{9}{4}, 3, \frac{1}{\xi^2}\right) \right\} dz', \end{aligned} \quad (15)$$

and

$$\begin{aligned} B_z &= \frac{1}{\rho} \frac{\partial(\rho A_\phi)}{\partial \rho}, \\ &= \frac{\mu_0 N_t I_0}{16\sqrt{2}\rho^{\frac{3}{2}}} \int_0^L \frac{1}{\sqrt{\rho'}\xi^{\frac{5}{2}}} \left\{ 5(\rho'\xi - \rho) F\left(\frac{3}{4}, \frac{9}{4}, 2, \frac{1}{\xi^2}\right) - (\rho'\xi - 2\rho) F\left(\frac{3}{4}, \frac{5}{4}, 2, \frac{1}{\xi^2}\right) \right\} dz'. \end{aligned} \quad (16)$$

Equations (15) and (16) can be rewritten in a number of different ways, and some of which may have better numerical properties than others. Eqs. (17) through (22) yield a few equivalent expressions for the radial and axial components of the magnetic flux density. These can be rigorously substantiated [23].

A few equivalent expressions for the radial components of the magnetic flux density produced by a thin conical current sheet are given as follows:

$$B_\rho = \frac{\mu_0 N_t I_0}{2} \int_0^L \int_0^\infty \rho' u J_1(\rho u) J_1(\rho' u) \operatorname{sgn}(z - z') e^{-u|z - z'|} du dz', \quad (17)$$

$$B_\rho = \frac{\mu_0 N_t I_0}{2\pi \rho^{\frac{3}{2}}} \int_0^L \frac{(z - z')}{\sqrt{\rho'}(1 - k^2)^2} \left\{ 2k^2 Q_{-\frac{1}{2}}(\xi) - k(1 + k^2) Q_{\frac{1}{2}}(\xi) \right\} dz', \quad (18)$$

$$B_\rho = \frac{\mu_0 N_t I_0}{\pi \rho} \int_0^L \frac{(z - z')}{l_2(1 - k^2)^2} \left\{ (1 + k^2) E(k^2) - (1 - k^2) K(k^2) \right\} dz'. \quad (19)$$

The addition of the term $\operatorname{sgn}(z - z') = \frac{d}{dz}|z - z'|$ in Eq. (17) is used in order to get the correct *sign* associated with B_ρ . The function $\operatorname{sgn}(z - z')$ is the signum function which is positive when its argument positive and negative when its argument is negative. In Mathematica [5], the signum function is represented by *Sign*(·).

Likewise, a few equivalent expressions for the axial components of the magnetic flux density produced by a thin conical current sheet are given by

$$B_z = \frac{\mu_0 N_t I_0}{2} \int_0^L \int_0^\infty \rho' u J_0(\rho u) J_1(\rho' u) e^{-u|z - z'|} du dz', \quad (20)$$

$$B_z = \frac{\mu_0 N_t I_0 \sqrt{\rho}}{\pi} \int_0^L \frac{\rho'^{\frac{3}{2}}}{l_2^4(1 - k^2)^2} \left\{ (\rho' \xi - \rho) Q_{-\frac{1}{2}}(\xi) + (\rho \xi - \rho') Q_{\frac{1}{2}}(\xi) \right\} dz', \quad (21)$$

$$B_z = \frac{\mu_0 N_t I_0}{\pi} \int_0^L \left\{ \frac{l_2^2 - \rho'^2}{l_2^3(1 - k^2)} K(k^2) - \frac{(z - z')^2 + \rho^2 - \rho'^2}{l_2^3(1 - k^2)^2} E(k^2) \right\} dz'. \quad (22)$$

The following expressions found in Eqs. (18), (19), (21) and (22) are defined as follows:

$$l_1 = \frac{1}{2} \left[\sqrt{(\rho + \rho')^2 + (z - z')^2} - \sqrt{(\rho - \rho')^2 + (z - z')^2} \right], \quad (23)$$

$$l_2 = \frac{1}{2} \left[\sqrt{(\rho + \rho')^2 + (z - z')^2} + \sqrt{(\rho - \rho')^2 + (z - z')^2} \right], \quad (24)$$

and

$$k = \frac{l_1}{l_2}. \quad (25)$$

The functions $K(\cdot)$ and $E(\cdot)$ are the complete elliptic integrals of the first and second kind, respectively. Also, $J_0(\cdot)$ and $J_1(\cdot)$ are Bessel functions of the first kind of order zero and one, respectively. Within the Mathematica [5] environment, the complete elliptic integrals of the first and second kind are expressed as *EllipticK* and *EllipticE*, respectively. Likewise, the Bessel function of the first kind is expressed as *BesselJ*.

Equations (17) through (19) can each be numerically checked against Eq. (13) or Eq. (15), and Eqs. (20) through (22) can each be numerically checked against Eq. (12) or Eq. (16). One must remember that in all expressions, ρ' is given by Eq. (5). In other words, the cylindrical source radius, ρ' , varies with the source axial variable, z' .

2.1.2. Magnetic Flux Density in Non-Integral Form

The radial and axial components of the magnetic flux density, in non-integral form, are found by integrating the expressions given by Eqs. (15) and (16). The non-integral expressions are then numerically checked against those given in integral form in Section 3.

a. Radial Component The radial component of the magnetic flux density is

$$B_\rho = \frac{\mu_0 N_t I_0 \rho R^3}{4\kappa L_{01}^5} \sum_{n=0}^{\infty} \frac{(4n+3)(4n+1)!!}{(2n+3)(n+1)!n!} \left(\frac{R\rho}{2L_{01}^2}\right)^{2n} \left\{ zF_{A0} - (z-L) \left(\frac{r}{R}\right)^{2n+3} \left(\frac{L_{01}}{L_{11}}\right)^{4n+5} F_{AL} \right. \\ \left. - \frac{R}{(2n+4)\kappa L_{01}^2} \times \left[a_1 \text{Re}[G_{A0}] - \frac{b_1}{\chi} \text{Im}[G_{A0}] \right. \right. \\ \left. \left. + \left(\frac{R-L\kappa}{R}\right) \left(\frac{r}{R}\right)^{2n+3} \left(\frac{L_{01}}{L_{11}}\right)^{4n+7} \left(a_2 \text{Re}[G_{AL}] - \frac{b_2}{\chi} \text{Im}[G_{AL}] \right) \right] \right\}, \quad (26)$$

where

$$a_1 = R(R - \kappa z) - z(z + \kappa R) + \rho^2, \quad (27)$$

$$b_1 = R^3\kappa + z^3\kappa^2 - R^2z(-2 + \kappa^2) + z\rho^2(2 + \kappa^2) + R\kappa(-3z^2 + \rho^2), \quad (28)$$

$$a_2 = -(R - 2\kappa L)[R - \kappa(z - L)] + (z - L)[(z - L) + \kappa R] - \kappa^2 L^2 - \rho^2, \quad (29)$$

$$b_2 = -R^3\kappa - z^3\kappa^2 + R^2z(-2 + \kappa^2) - L^2\kappa(R - z\kappa)(1 + \kappa^2) - z\rho^2(2 + \kappa^2) \\ - R\kappa(-3z^2 + \rho^2) + 2L(1 + \kappa^2)(R^2 - Rz\kappa + \rho^2). \quad (30)$$

b. Axial Component The axial component of the magnetic flux density is given by

$$B_z = \frac{\mu_0 N_t I_0 R^3}{4\kappa L_{01}^5} \sum_{n=0}^{\infty} \frac{(4n+1)!!}{(2n+3)(n+1)!n!} \left(\frac{R\rho}{2L_{01}^2}\right)^{2n} \left\{ [(2n+2)L_{02}^2 + \rho^2] F_{A0} - \left(\frac{r}{R}\right)^{2n+3} \right. \\ \times \left(\frac{L_{01}}{L_{11}}\right)^{4n+5} [(2n+2)L_{12}^2 + \rho^2] F_{AL} - \frac{(4n+3)\rho^2}{(2n+4)\kappa} \left[\frac{R}{L_{01}^2} \left(a_1 \text{Re}[G_{A0}] - \frac{b_1}{\chi} \text{Im}[G_{A0}] \right) \right. \\ \left. \left. - \left(\frac{r}{R}\right)^{2n+3} \left(\frac{L_{01}}{L_{11}}\right)^{4n+5} \left(\frac{R-L\kappa}{L_{11}^2}\right) \left(a_2 \text{Re}[G_{AL}] - \frac{b_2}{\chi} \text{Im}[G_{AL}] \right) \right] \right\}, \quad (31)$$

where

$$a_1 = 2(z + R\kappa), \quad (32)$$

$$b_1 = (z + R\kappa)^2 - \chi^2, \quad (33)$$

$$a_2 = 2[(z + R\kappa) - L(1 + \kappa^2)], \quad (34)$$

$$b_2 = [(z + R\kappa) - L(1 + \kappa^2)]^2 - \chi^2. \quad (35)$$

For both the radial and axial components of the magnetic flux density, the following expressions are needed.

$$\chi = \sqrt{(R - \kappa z)^2 + (1 + \kappa^2)\rho^2}, \quad (36)$$

$$L_{01} = \sqrt{R^2 + z^2 + \rho^2}, \quad (37)$$

$$L_{11} = \sqrt{(R - L\kappa)^2 + (z - L)^2 + \rho^2}, \quad (38)$$

$$L_{02} = \sqrt{R^2 + z^2 - \rho^2}, \quad (39)$$

$$L_{12} = \sqrt{(R - L\kappa)^2 + (z - L)^2 - \rho^2}, \quad (40)$$

and

$$F_{AL} = F_A \left[1, 2n + \frac{3}{2}, 2n + \frac{3}{2}, 2n + 4, \frac{x_1}{x_1 - 1}, \frac{y_1}{y_1 - 1} \right], \tag{41}$$

$$F_{A0} = F_A \left[1, 2n + \frac{3}{2}, 2n + \frac{3}{2}, 2n + 4, \frac{x_2}{x_2 - 1}, \frac{y_2}{y_2 - 1} \right], \tag{42}$$

$$G_{AL} = G_A \left[2, 2n + \frac{3}{2}, 2n + \frac{5}{2}, 2n + 5, \frac{x_1}{x_1 - 1}, \frac{y_1}{y_1 - 1} \right], \tag{43}$$

$$G_{A0} = G_A \left[2, 2n + \frac{3}{2}, 2n + \frac{5}{2}, 2n + 5, \frac{x_2}{x_2 - 1}, \frac{y_2}{y_2 - 1} \right]. \tag{44}$$

Also,

$$x_1 = \frac{(R - L\kappa)(1 + \kappa^2)}{(R - \kappa z) + i\kappa\chi}, \tag{45}$$

$$y_1 = \frac{(R - L\kappa)(1 + \kappa^2)}{(R - \kappa z) - i\kappa\chi}, \tag{46}$$

$$x_2 = \frac{R(1 + \kappa^2)}{(R - \kappa z) + i\kappa\chi}, \tag{47}$$

$$y_2 = \frac{R(1 + \kappa^2)}{(R - \kappa z) - i\kappa\chi}. \tag{48}$$

Equations (41) through (44) are defined as *Appell hypergeometric functions* [6, 24, 25] and are expressed in Mathematica [5] as *AppellF1*. Also, $i = \sqrt{-1}$. Although the denominators in Eqs. (45) through (48) are complex-valued functions, all magnetic field computations evaluate to real quantities.

2.2. Conical Coil Model

The conical coil model is illustrated in Fig. 2 as viewed from the x axis. Also, the current is flowing in a purely azimuthal direction. The chosen model assumes that the pitch of each coil is zero. Although each

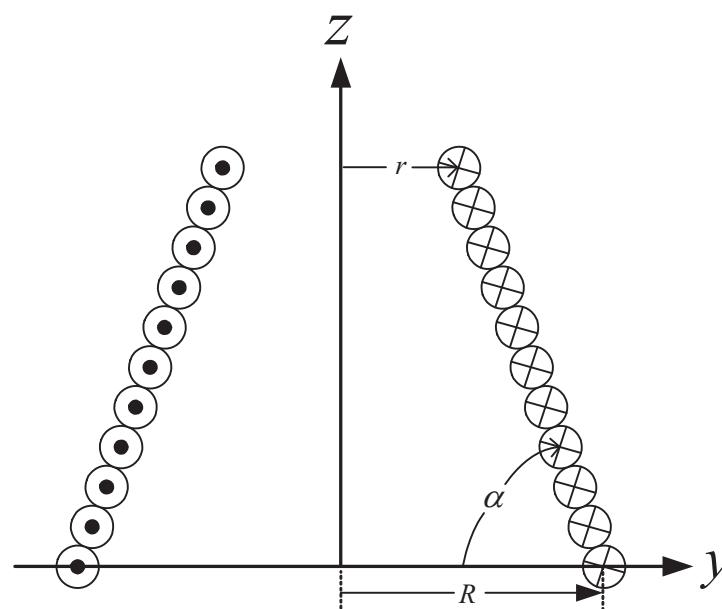


Figure 2. Thin conical coil.

coil must have a cross-sectional area, the authors assume that this has a negligible effect as previously discussed in the introduction of this article.

The magnetic flux density produced by a tightly-wound conical coil is found by revisiting Eq. (18) or Eq. (19), and Eq. (21) or Eq. (22). The radial and axial components of the magnetic flux density in terms of toroidal harmonics are

$$B_\rho = \frac{\mu_0 I_0}{2\pi\rho^{\frac{3}{2}}} \left\{ \frac{z}{\sqrt{R}(1-k_{coil_0}^2)^2} \left[2k_{coil_0}^2 Q_{-\frac{1}{2}}(\xi_{coil_0}) - k_{coil_0}(1+k_{coil_0}^2) Q_{\frac{1}{2}}(\xi_{coil_0}) \right] \right. \\ \left. + \sum_{m=1}^{M-1} \frac{(z-mh)}{\sqrt{R-m\Delta}(1-k_{coil}^2)^2} \left[2k_{coil}^2 Q_{-\frac{1}{2}}(\xi_{coil}) - k_{coil}(1+k_{coil}^2) Q_{\frac{1}{2}}(\xi_{coil}) \right] \right\}, \quad (49)$$

and

$$B_z = \frac{\mu_0 I_0 \sqrt{\rho}}{\pi} \left\{ \frac{R^{\frac{3}{2}}}{l_{2coil_0}^4 (1-k_{coil_0}^2)^2} \left[(R\xi_{coil_0} - \rho) Q_{-\frac{1}{2}}(\xi_{coil_0}) + (\rho\xi_{coil_0} - R) Q_{\frac{1}{2}}(\xi_{coil_0}) \right] \right. \\ \left. + \sum_{m=1}^{M-1} \frac{(R-m\delta)^{\frac{3}{2}}}{l_{2coil}^4 (1-k_{coil}^2)^2} \left([(R-m\Delta)\xi_{coil} - \rho] Q_{-\frac{1}{2}}(\xi_{coil}) + [\rho\xi_{coil} - (R-m\delta)] Q_{\frac{1}{2}}(\xi_{coil}) \right) \right\}. \quad (50)$$

Likewise, the same components can be written in terms of elliptic integrals as follows:

$$B_\rho = \frac{\mu_0 I_0}{\pi\rho} \left\{ \frac{z}{l_{2coil_0} (1-k_{coil_0}^2)} \left[\frac{1+k_{coil_0}^2}{1-k_{coil_0}^2} E(k_{coil_0}^2) - K(k_{coil_0}^2) \right] + \sum_{m=1}^{M-1} \frac{z-mh}{l_{2coil} (1-k_{coil}^2)} \times \right. \\ \left. \left[\frac{1+k_{coil}^2}{1-k_{coil}^2} E(k_{coil}^2) - K(k_{coil}^2) \right] \right\}, \quad (51)$$

$$B_z = \frac{\mu_0 I_0}{\pi} \left\{ \left[\frac{l_{2coil_0}^2 - R^2}{l_{2coil_0}^3 (1-k_{coil_0}^2)} K(k_{coil_0}^2) - \frac{z^2 + \rho^2 - R^2}{l_{2coil_0}^3 (1-k_{coil_0}^2)^2} E(k_{coil_0}^2) \right] \right. \\ \left. + \sum_{m=0}^{M-1} \left(\frac{[l_{2coil}^2 - (R-m\delta)^2]}{l_{2coil}^3 (1-k_{coil}^2)} K(k_{coil}^2) - \frac{(z-mh)^2 + \rho^2 - (R-m\delta)^2}{l_{2coil}^3 (1-k_{coil}^2)^2} E(k_{coil}^2) \right) \right\}, \quad (52)$$

where

$$\xi_{coil} = \frac{\rho^2 + (R-m\delta)^2 + (z-mh)^2}{2\rho(R-m\delta)}, \quad (53)$$

and

$$k_{coil} = \frac{l_{1coil}}{l_{2coil}}. \quad (54)$$

The expressions for l_{1coil} and l_{2coil} are given by Eqs. (23) and (24) with ρ' replaced with $R-m\delta$, and z' replaced with mh . Also, the authors define the following quantities as

$$\delta = \frac{R-r}{M-1}, \quad (55)$$

and

$$h = \frac{L}{M-1}, \quad (56)$$

where $M = N_t L$ is the total number of coils assumed to be an integer value. Of course, this requires the reader to choose a length L which forces $N_t L$ to be whole number. This requirement is only made in order to make a direct comparison to that of the conical current sheet.

The index $m = 0$ corresponds to the location of the first circular coil at a radius R at the base of the frustum at the $z = 0$ plane, and the index $m = M - 1$ corresponds to the location of the last circular coil at a radius r at the top of the frustum at $z = L$. Therefore, ξ_{coil_0} , k_{coil_0} , and $l_{2_{coil_0}}$ are those values of ξ_{coil} , k_{coil} , and $l_{2_{coil}}$ evaluated at $m = 0$. The symbol, δ , represents the change in the radial length of each coil from R to r as m goes from 0 to $M - 1$ for a total of M coils. Also, h is the change in height of the observation point for each coil above the $z = 0$ plane.

The defining equations for δ and h are used so as to make a more reasonable comparison between the conical current sheet and the conical coil while maintaining a uniform current I_0 . The authors are not attempting to find an equivalent current density of the conical coil which will yield the same magnetic field at some observation point as that produced by conical current sheet. The main idea is to simply make a direct comparison between the two structures while maintaining the same number of turns per unit length, N_t , for both the conical current sheet and the conical coil [7]. However, one may devise alternative ways to make comparisons which may depend on the type of application.

The authors have also assumed that each coil completes a full turn. In other words, when comparing the magnetic field from a conical coil to that of a conical current sheet, the authors have assumed that the conical coil is made up of M complete coils. Remember, the above formulas were ultimately derived from Eqs. (12) and (13) leading to the expressions given by Eq. (18) or Eq. (19), and Eq. (21) or Eq. (22), and where all integrations were replaced with summations. The azimuthal integration for all expressions was from 0 to 2π . If a partial turn of a coil is to be considered then one would need to change the upper limit of 2π to a value which corresponds to the non-integral turn of a coil. This, of course, can easily be done. However, all derived expressions would no longer be azimuthally symmetric. In other words, there would be a ϕ variation in the mathematical expressions for the magnetic field. This would result in a B_ϕ component. This ϕ component would come from that coil with the non-integral turn. Of course, one could always add this separately using superposition.

3. NUMERICAL AND GRAPHICAL ANALYSIS

A number of numerical examples are given to test the mathematical expressions developed in Section 2. The authors will work with the magnetic field intensity, \mathbf{H} , instead of the magnetic flux density, \mathbf{B} , for all subsequent analysis in order to keep the numerical values at a more reasonable size. The units of magnetic field intensity used for all examples is A/m . A series of tables illustrating various computational results as well as various plots will be developed in this section. Also, the current I_0 will be set to unity for all examples.

Equations (15), (18), and (19), within the Mathematica [5] environment, give excellent numerical results for the radial component of the magnetic flux density. The numerical integration of these three equations appear to be extremely robust. The same holds true for the axial component of the magnetic flux density given by Eqs. (16), (21) and (22). The authors will choose both Eqs. (18) and (21) as the benchmark for comparison in all subsequent numerical analysis.

The numerical integration of Eqs. (18) and (21) will produce a single value and it is independent of the index n as illustrated in column 1 in each table developed in this section. Also, n_{\max} , in column 2 of each table is the maximum value of the index used in the summation of Eq. (26) or Eq. (31). The percent difference used in column 4 is the absolute value of the difference between column 1 and column 3 divided by the absolute value of column 1, where the result is given as a percentage. As the index n increases, the $\% \Delta$ can be made as small as desired. In general, the closer the observation point is to the magnetic source, the more terms in the series of Eq. (26) or Eq. (31) will be required to reduce the $\% \Delta$ to a desired value. This is not unusual.

As the observation point moves farther from the magnetic source, fewer and fewer terms in the series solution of Eq. (26) or Eq. (31) will be needed. This is also not at all surprising. The authors will illustrate the numerical equivalence for a number of equations given in Section 2 as well as their analytical counterparts given by Eqs. (26) and (31). Our aim is to give the reader multiple options in modeling conical current sheets and thin and tightly-wound conical coils. Depending upon the application, one formulation may be more advantageous than another.

3.1. Example 1

Consider the conically-shaped current sheet of Fig. 1 with the following geometric data.

$L = 1.0 \text{ inch} = 0.0254 \text{ m}$	$R = 3.0 \text{ inches} = 0.0762 \text{ m}$
$r = \frac{1}{4} \text{ inch} = 0.00635 \text{ m}$	$N_t = 25 \frac{\text{turns}}{\text{in}} = 984.25 \frac{\text{turns}}{\text{m}}$

Find the radial component, H_ρ , of the magnetic field intensity at an observation height of $z = 1.25$ in or 0.03175 m and at an observation radius of $\rho = 0.125$ in or 0.003175 m. Employ numerical integration on Eq. (18) and compare the results to those obtained from a direct evaluation of Eq. (26). The results are tabulated in Table 1.

Table 1. Comparison between numerical integration of Eq. (18) and its analytical counterpart given by Eq. (26).

<i>Numerical Integration</i> $\mu_0^{-1} \times \text{Eq. (18)}$	n_{\max}	$H_\rho = \frac{B_\rho}{\mu_0}$ $\mu_0^{-1} \times \text{Eq. (26)}$	$\% \Delta$
30.575933	0	27.199708	11.0421
.	2	30.501109	0.24471
.	4	30.573828	0.00688
.	6	30.575868	0.00021
30.575933	8	30.575931	6.89009×10^{-6}

Now, find the axial component, H_z , of the magnetic field intensity at an observation height of $z = 1.25$ in or 0.03175 m and at an observation radius of $\rho = 0.125$ in or 0.003175 m. Employ numerical integration on Eq. (21) and compare the results to those obtained from a direct evaluation of Eq. (31). The results are tabulated in Table 2.

Table 2. Comparison between numerical integration of Eq. (21) and its analytical counterpart given by Eq. (31).

<i>Numerical Integration</i> $\mu_0^{-1} \times \text{Eq. (21)}$	n_{\max}	$H_z = \frac{B_z}{\mu_0}$ $\mu_0^{-1} \times \text{Eq. (31)}$	$\% \Delta$
279.736832	0	265.074994	5.2413
.	2	279.527348	0.0749
.	4	279.731709	0.0018
.	6	279.736685	0.0001
279.736832	8	279.736827	1.6330×10^{-6}

3.2. Example 2

Figures 3 and 4 compare two plots of the radial component of the magnetic field intensity, H_ρ , as a function of the axial variable, z . The geometric data used is that from Example 1. The observation radius chosen is $\rho = 0.125$ in or 0.003175 m. Eq. (18) is compared to Eq. (26). The maximum value of the index used in Eq. (26) in Fig. 3 is $n_{\max} = 0$. This value of n at an observation radius of $\rho = 0.003175$ m and at a height of $z = 0.03175$ m corresponds to a $\% \Delta$ of about 11.0% as seen from Table 1. The maximum value of the index used in Eq. (26) in Fig. 4 is $n_{\max} = 2$. This value of n at an observation radius of $\rho = 0.003175$ m and at a height of $z = 0.03175$ m corresponds to a $\% \Delta$ of about 0.24% as seen

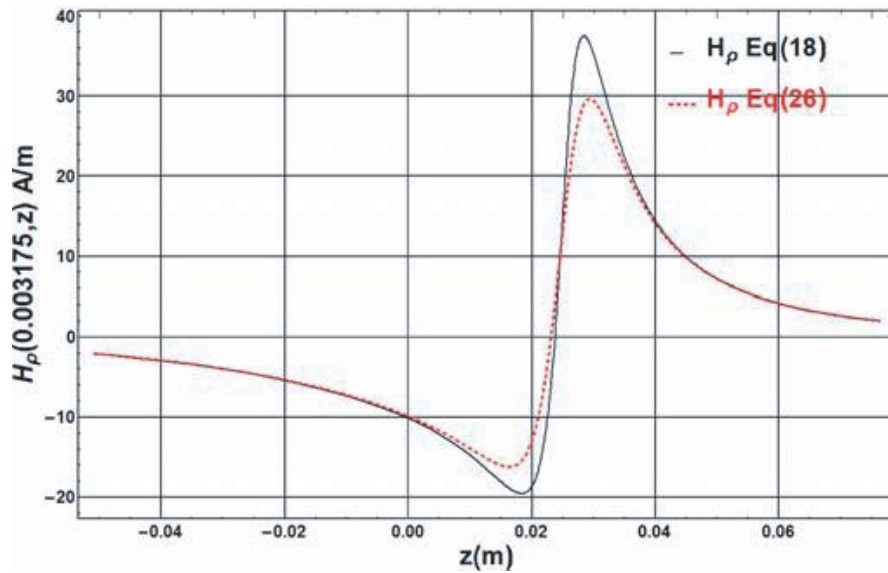


Figure 3. H_ρ at $\rho = 0.003175$ m versus the axial height, z . The maximum index used in Eq. (26) is $n = 0$.

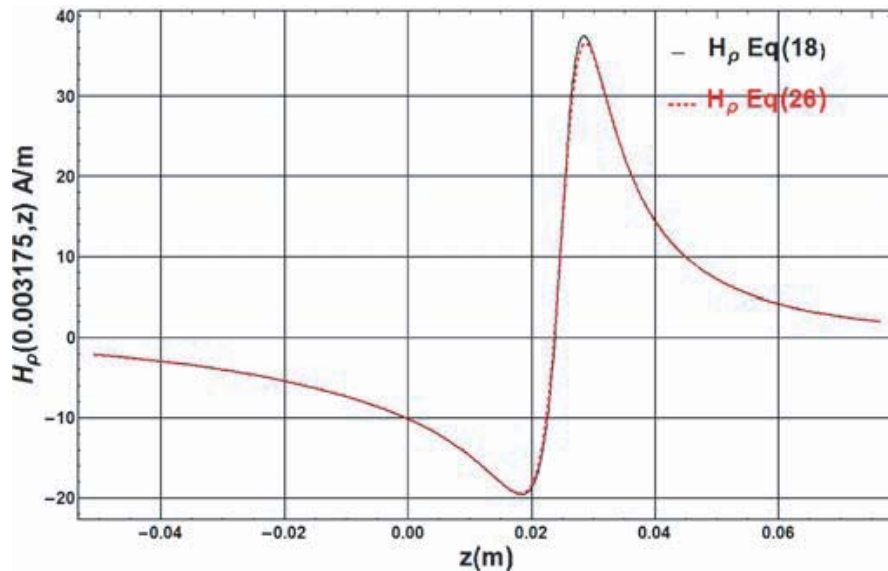


Figure 4. H_ρ at $\rho = 0.003175$ m versus the axial height, z . The maximum index used in Eq. (26) is $n = 2$.

from Table 1. A detailed error analysis would need to be performed if one were more interested in how Eqs. (18) and (26) compare as the index n increases.

Figures 5 and 6 compare two plots of the axial component of the magnetic field intensity, H_z , as a function of the radial variable, ρ . Once again, the geometric data used is that from Example 1. The observation height is chosen to be $z = 1.25$ in or 0.03175 m. Eq. (21) is compared to Eq. (31). The maximum value of the index used in Eq. (31) in Fig. 5 is $n_{\max} = 0$. This value of n at an observation height of $z = 0.03175$ m and at an observation radius of $\rho = 0.003175$ m corresponds to a $\% \Delta$ of about 5.2% as seen from Table 2. The maximum value of the index used in Eq. (31) for Fig. 6 is $n_{\max} = 8$. This value of n at an observation height of $z = 0.03175$ m and at an observation radius of $\rho = 0.003175$ m corresponds to a $\% \Delta$ of about $1.6 \times 10^{-6}\%$ as seen from Table 2.

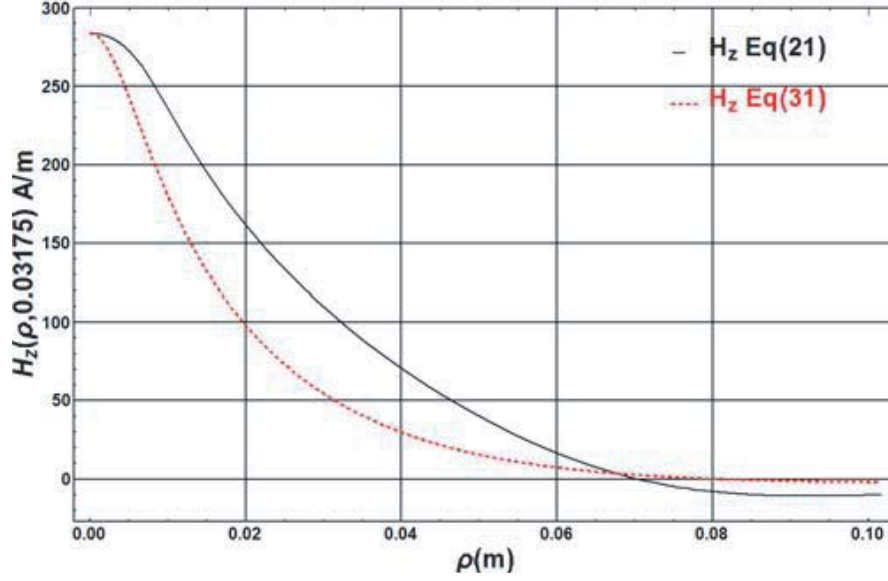


Figure 5. H_z at $z = 0.03175$ m versus the observation radius, ρ . The maximum index used in Eq. (31) is $n = 0$.

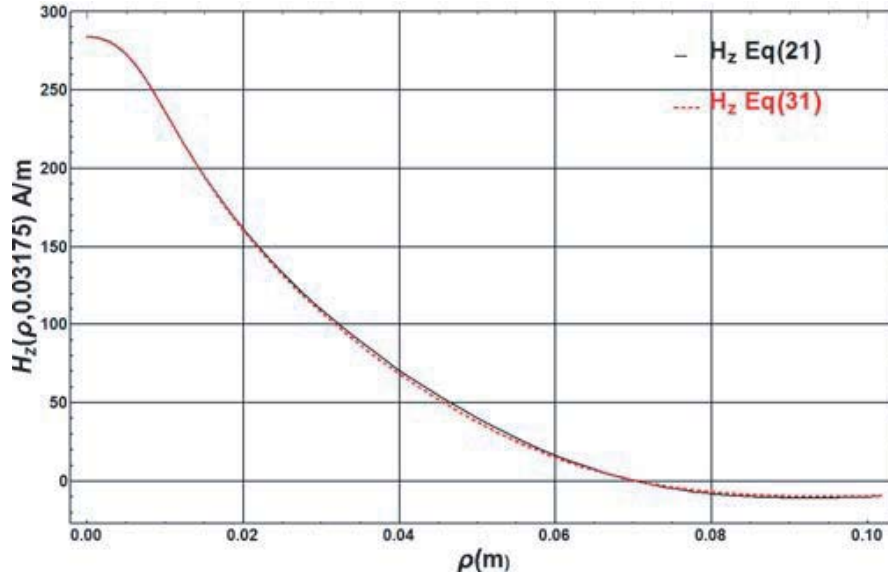


Figure 6. H_z at $z = 0.03175$ m versus the observation radius, ρ . The maximum index used in Eq. (31) is $n = 8$.

The next example will illustrate a comparison between the conical current sheet and the conical coil for the same turns per unit length, N_t , and the same current, I_0 .

3.3. Example 3

The geometric data from Example 1 are used for this example. Fig. 7 compares the plots of Eqs. (18) and (49) for radial observation point of $\rho = 0.125$ in or 0.003175 m as a function of the axial variable, z . Fig. 8 compares the plots of Eqs. (21) and (50) for axial observation height of $z = 1.25$ in or 0.03175 m as a function of the radial variable, ρ . The data given for Example 1 yields a total of 25 coils.

Example 3 compares the conical current sheet model to the conical coil model. One should not

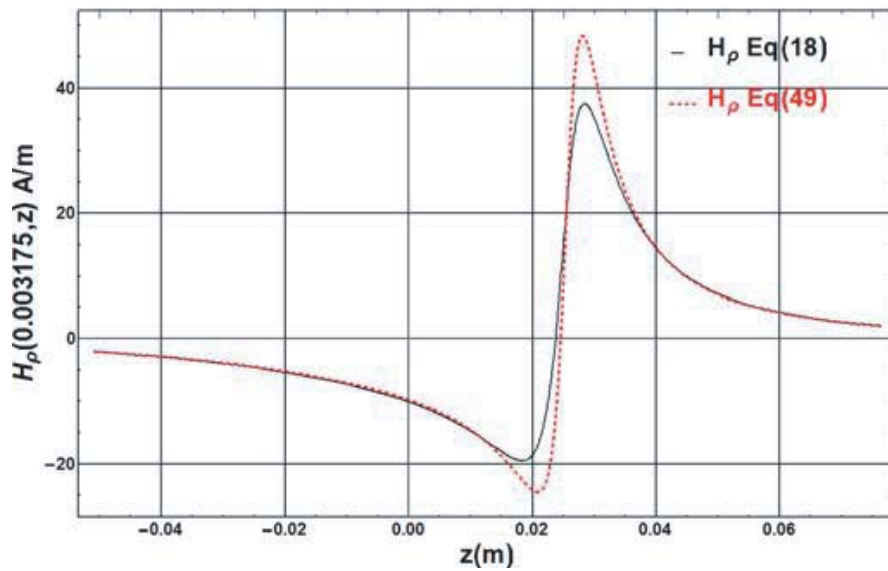


Figure 7. H_ρ at $\rho = 0.003175$ m versus the axial height, z .

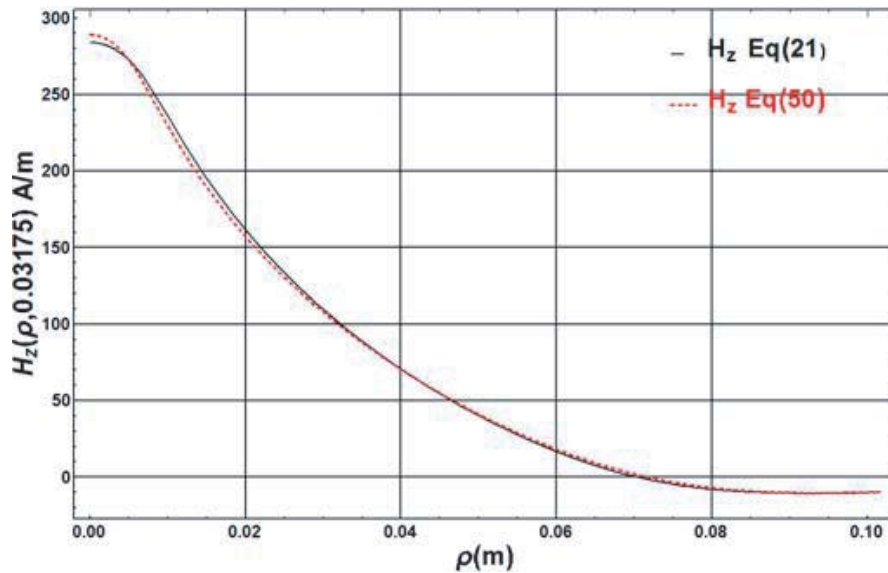


Figure 8. H_z at $z = 0.03175$ m versus the observation radius, ρ .

expect both plots to be identical since the current sheet model takes into account a continuum of source values through the integration of the z' source variable, whereas the coil model takes into account only a finite number of coils through a finite summation process. What is certainly shown is that if one were interested in computing the magnetic field from a conical current sheet, it may be advantageous to use the coil model to get a good idea of the shape of the magnetic field. The coil model has the advantage that no integrations need to be performed and only a finite sum is needed.

The main difference in the value of the magnetic field due to the conical current sheet versus the conical coil will be at those observation points where a larger magnetic field gradient exists. The coil model and the current-sheet model may produce very similar magnetic field values depending upon where the observation point is located.

If one is designing a conical coil then one would want to directly employ the conical coil equations

given that the assumptions stated in the introduction section of this article are deemed acceptable. If a conical coil is designed, and if the pitch of the coil becomes relevant, then the conical coil model introduced in this article must be modified to include the helical structure of the coil [2]. Modeling the helical structure of the coil can be done, but the mathematics becomes more involved.

4. CYLINDRICAL CURRENT SHEET

The magnetic field produced by a conical current sheet can be employed to find the magnetic field from a finite cylindrical current sheet. This allows for a direct comparison with published results, and is just another validation of the equations developed in Section 2. Consider the ideal geometric model chosen for a thin and cylindrically-shaped current sheet illustrated in Fig. 9. This model is the limiting case as $\alpha \rightarrow \frac{\pi}{2}$ for the conically-shaped current sheet shown in Fig. 1. This implies that $r \rightarrow R$ in the conical current sheet model.

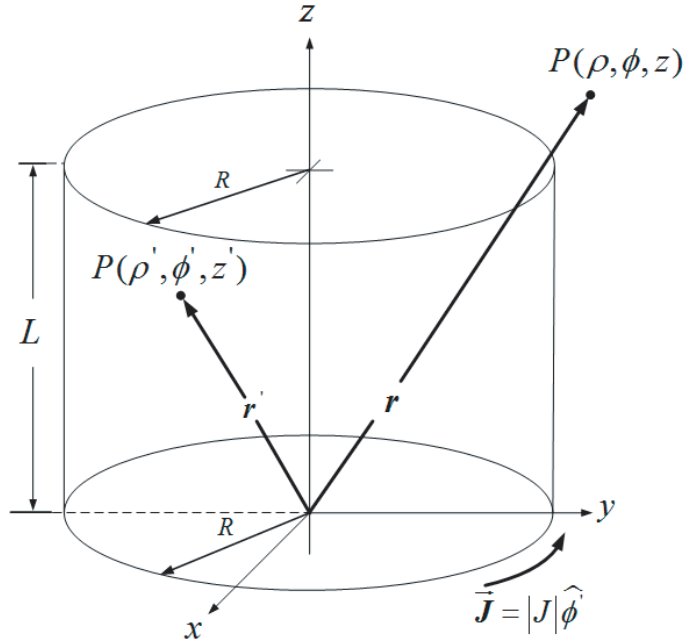


Figure 9. Cylindrical current sheet.

4.1. Magnetic Flux Density in Integral Form

In the limiting case as $\kappa \rightarrow 0$ or as $r \rightarrow R$, the mathematical expressions in Section 2 will degenerate to those of a thin cylindrical current sheet or an infinitely-thin cylindrical coil. For example, consider the radial component of the magnetic flux density given by Eq. (18) as $\kappa \rightarrow 0$.

$$B_\rho = \frac{\mu_0 N_t I_0}{2\pi\sqrt{R}\rho^{\frac{3}{2}}} \int_0^L \frac{(z - z')}{(1 - k^2)^2} \left\{ 2k^2 Q_{-\frac{1}{2}}(\xi) - k(1 + k^2) Q_{\frac{1}{2}}(\xi) \right\} dz', \quad (57)$$

where ξ is given by

$$\xi = \frac{\rho^2 + R^2 + (z - z')^2}{2\rho R}. \quad (58)$$

Likewise, the axial component of the magnetic flux density given by Eq. (21) as $\kappa \rightarrow 0$ is given by

$$B_z = \frac{\mu_0 N_t I_0 R^{\frac{3}{2}} \sqrt{\rho}}{\pi} \int_0^L \frac{1}{l^4 (1 - k^2)^2} \left\{ (R\xi - \rho) Q_{-\frac{1}{2}}(\xi) + (\rho\xi - R) Q_{\frac{1}{2}}(\xi) \right\} dz'. \quad (59)$$

In Eqs. (58) and (59), k is given by Eq. (25) with l_1 and l_2 given by Eqs. (23) and (24) but with ρ replaced by R . All other expressions for the magnetic flux density due to a thin conical current sheet, developed in Section 2.1, can be rewritten for the thin cylindrical current sheet by letting $\kappa \rightarrow 0$.

4.2. Magnetic Flux Density in Non-Integral Form

When $\kappa \rightarrow 0$, the vector potential given by Eq. (14) can be directly integrated in terms of complete elliptic integrals of the first, second and third kind. This yields the following magnetic vector potential.

$$A_\phi = \frac{\mu_0 N_t I_0}{2\pi} \sqrt{\frac{R}{\rho}} \left\{ z k_0 \left[\left(\frac{k_0^2 + \beta^2 (1 - k_0^2)}{\beta^2 k_0^2} \right) \mathbf{K}(k_0^2) - \frac{\mathbf{E}(k_0^2)}{k_0^2} + \frac{\beta^2 - 1}{\beta^2} \Pi(\beta^2, k_0^2) \right] - (z - L) k_L \left[\left(\frac{k_L^2 + \beta^2 (1 - k_L^2)}{\beta^2 k_L^2} \right) \mathbf{K}(k_L^2) - \frac{\mathbf{E}(k_L^2)}{k_L^2} + \frac{\beta^2 - 1}{\beta^2} \Pi(\beta^2, k_L^2) \right] \right\}, \quad (60)$$

where

$$\beta^2 = \frac{4R\rho}{(\rho + R)^2}, \quad (61)$$

$$k_0^2 = \frac{4R\rho}{(R + \rho)^2 + z^2}, \quad (62)$$

$$k_L^2 = \frac{4R\rho}{(R + \rho)^2 + (z - L)^2}. \quad (63)$$

The function $\Pi(\cdot)$ is defined as the complete elliptic integral of the third kind, and this is expressed in Mathematica [5] as *EllipticPi*. One caveat in the application of Eq. (60) is that when the observation radius $\rho = R$ or $\beta^2 = 1$, which results in two evaluations of the elliptic integral of the third kind, the elliptic integral of the third kind becomes undefined. However, in the limit as $\rho \rightarrow R$, $(\beta^2 - 1)\Pi(\beta^2, k_0^2)$ and $(\beta^2 - 1)\Pi(\beta^2, k_L^2)$ both are finite and approach zero. As long as the source point and the observation point are not coincident, the magnetic field is non-singular. When evaluating the elliptic integral of the third kind for circular intervals of the parameter, β^2 , it is usually rewritten in terms of the Heuman lambda function. The details of this can be found in Byrd and Friedman [26]. The authors chose not to employ this technique. However, a number of authors cited in this article have taken this approach.

Employing Eq. (60) and the $[\nabla \times \mathbf{A}]_z$ yields the radial component of the magnetic flux density, B_ρ , given by [27]

$$B_\rho = -\frac{\partial A_\phi}{\partial z}, \\ = \frac{\mu_0 N_t I_0}{\pi} \sqrt{\frac{R}{\rho}} \left\{ \frac{2 - k_L^2}{2k_L} \mathbf{K}(k_L^2) - \frac{2 - k_0^2}{2k_0} \mathbf{K}(k_0^2) + \frac{\mathbf{E}(k_0^2)}{k_0} - \frac{\mathbf{E}(k_L^2)}{k_L} \right\}. \quad (64)$$

An alternate form for the radial component of the magnetic flux density can be written as follows:

$$B_\rho = \frac{\mu_0 N_t I_0 R^2 \rho}{4} \left\{ \frac{F_G \left[\left\{ \frac{3}{4}, \frac{5}{4} \right\}, \{2\}, \frac{1}{\xi_L^2} \right]}{(R^2 + (z - L)^2 + \rho^2)^{\frac{3}{2}}} - \frac{F_G \left[\left\{ \frac{3}{4}, \frac{5}{4} \right\}, \{2\}, \frac{1}{\xi_0^2} \right]}{(R^2 + z^2 + \rho^2)^{\frac{3}{2}}} \right\}, \quad (65)$$

where $F_G(\cdot)$ is the *generalized hypergeometric function* [28], and it is expressed in Mathematica [5] as *HypergeometricPFQ*. Also, the following expressions in Eq. (65) are defined as

$$\xi_L = \frac{R^2 + (z - L)^2 + \rho^2}{2R\rho}, \quad (66)$$

and

$$\xi_0 = \frac{R^2 + z^2 + \rho^2}{2R\rho}. \quad (67)$$

Equation (65) is not in a form often found in the literature. Often one finds elliptic integral expressions when dealing with cylindrical geometries. Eqs. (64) and (65) are both valid for all observation points external to the current source. Eq. (64) matches that found by Conway [29]. Both expressions given by Eqs. (64) and (65) yield identical numerical results in Mathematica [5]. However, whether (64) or (65) is more numerically robust has not been addressed by the authors. Eqs. (64) and (65) are not unique. One can find other expressions which are mathematically equivalent. In fact, the interested reader may want to express the elliptic integral formulations for the radial and axial magnetic field components in terms of toroidal harmonics.

Employing Eq. (60) and the $[\nabla \times \mathbf{A}]_\rho$ [30] yields the axial component of the magnetic flux density, B_z , given by

$$\begin{aligned} B_z &= \frac{1}{\rho} \frac{\partial(\rho A_\phi)}{\partial \rho}, \\ &= \frac{\mu_0 N_t I_0}{4\pi\sqrt{R\rho}} \left\{ z k_0 \left[\mathcal{K}(k_0^2) + \frac{R-\rho}{R+\rho} \Pi(\beta^2, k_0^2) \right] - (z-L) k_L \left[\mathcal{K}(k_L^2) + \frac{R-\rho}{R+\rho} \Pi(\beta^2, k_L^2) \right] \right\}. \end{aligned} \quad (68)$$

Alternatively, B_z can be put into the following mathematical form given by [27]

$$\begin{aligned} B_z &= \frac{\mu_0 N_t I_0}{4} \left\{ \frac{z k_0}{\pi\sqrt{\rho R}} \mathcal{K}(k_0^2) - \frac{(z-L) k_L}{\pi\sqrt{\rho R}} \mathcal{K}(k_L^2) + \text{sgn}[z(R-\rho)] \left[\frac{\mathcal{F}(\phi_0, 1-k_0^2)}{\mathcal{K}(1-k_0^2)} + \frac{2\mathcal{K}(k_0^2)\mathcal{Z}(\phi_0, 1-k_0^2)}{\pi} \right] \right. \\ &\quad \left. - \text{sgn}[(z-L)(R-\rho)] \left[\frac{\mathcal{F}(\phi_L, 1-k_L^2)}{\mathcal{K}(1-k_L^2)} + \frac{2\mathcal{K}(k_L^2)\mathcal{Z}(\phi_L, 1-k_L^2)}{\pi} \right] \right\}, \end{aligned} \quad (69)$$

where

$$\phi_0 = \tan^{-1} \left(\left| \frac{z}{R-\rho} \right| \right), \quad (70)$$

$$\phi_L = \tan^{-1} \left(\left| \frac{z-L}{R-\rho} \right| \right). \quad (71)$$

Also, $\mathcal{F}(\phi, 1-k^2)$ and $\mathcal{Z}(\phi, 1-k^2)$ are the incomplete elliptic integral of the first kind and the Jacobi zeta function, respectively. In Mathematica [5], the incomplete elliptic integral of the first kind is written as *EllipticF*, and the Jacobi zeta function is written as *JacobiZeta*. The numerical evaluation of Eq. (69) does not require a limit as $\rho \rightarrow R$ to evaluate the axial component of the magnetic field at $\rho = R$.

Equation (68) is a simpler-looking mathematical expression than Eq. (69) and yields identical results for all observation points. Also, Eq. (68) does not need to introduce the incomplete elliptic integral of the first kind or the Jacobi Zeta function, both of which can be rewritten in terms of the Heuman lambda function [26, 29]. In general, if a physical geometry exhibits some sort of symmetry about an axis, the mathematical expression for the magnetic field off the symmetry axis becomes much more complex, and its mathematical description usually requires the application of special functions.

Equations (68) and (69) agree numerically with the axial component of the magnetic flux density, B_z , published in Conway [29]. However, Conway [29] derives the axial component of the magnetic flux density in terms of the complete elliptic integral of the first kind and the Heuman lambda function for distinct observation regions. Using our notation, Conway [29] derives expressions for B_z valid for $z < 0$, for $0 < z < L$ and for $z > L$. However, Eqs. (68) and (69) are single mathematical expressions valid at all observation points external to the current source.

Recently, a number of authors have reintroduced methods for analytically evaluating the magnetic field and the inductance from circular cylindrical structures [31–49]. These same methods prove fruitful for developing the mathematical expressions needed for finding the magnetic field from conical structures. With the advent of powerful mathematical programs such as Mathematica [5], much of the algebraic intensive work necessary to handle the complex mathematics associated with magnetic field computations off the symmetry axis becomes much more accessible.

4.3. Numerical Analysis

Consider the cylindrically-shaped current sheet with the following data.

$L = 1.0 \text{ inch} = 0.0254 \text{ m}$
$R = 3.0 \text{ inches} = 0.0762 \text{ m}$
$N_t = 25 \frac{\text{turns}}{\text{in}} = 984.25 \frac{\text{turns}}{\text{m}}$

Find the radial component, H_ρ , of the magnetic field intensity at an observation radius of $\rho = 0.125 \text{ in}$ or 0.003175 m and for various observation heights. Employ numerical integration on Eq. (57) and compare the results to those obtained from a direct evaluation of Eqs. (64) and (65). The results are tabulated in Table 3.

Table 3. Comparison between numerical integration of Eq. (57) and its analytical counterpart given by Eq. (64) or Eq. (65).

ρ	z	Numerical Integration $\mu_0^{-1} \times \text{Eq. (57)}$	$H_\rho = \frac{B_\rho}{\mu_0}$ $\mu_0^{-1} \times \text{Eq. (64)}$	$H_\rho = \frac{B_\rho}{\mu_0}$ $\mu_0^{-1} \times \text{Eq. (65)}$
0.003175	0.03175	2.08795	2.08795	2.08795
.	0.02540	1.50290	1.50290	1.50290
.	0.01270	0.00000	0.00000	0.00000
.	0.00000	-1.50290	-1.50290	-1.50290
.	-0.0127	-2.50901	-2.50901	-2.50901
.	-0.0254	-2.85197	-2.85197	-2.85197
0.003175	-0.03175	-2.81753	-2.81753	-2.81753

Find the axial component, H_z , of the magnetic field intensity at an observation radius of $\rho = 0.125 \text{ in}$ or 0.003175 m and for various observation heights. Employ numerical integration on Eq. (59) and compare the results to those obtained from a direct evaluation of Eqs. (68) and (69). The results are tabulated in Table 4.

Table 4. Comparison between numerical integration of Eq. (59) and its analytical counterpart given by Eq. (68) or Eq. (69).

ρ	z	Integration Numerical $\mu_0^{-1} \times \text{Eq. (59)}$	$H_z = \frac{B_\rho}{\mu_0}$ $\mu_0^{-1} \times \text{Eq. (68)}$	$H_z = \frac{B_\rho}{\mu_0}$ $\mu_0^{-1} \times \text{Eq. (69)}$
0.003175	0.03175	148.53662	148.53662	148.53662
.	0.02540	155.78791	155.78791	155.78791
.	0.01270	162.00945	162.00945	162.00945
.	0.00000	155.78791	155.78791	155.78791
.	-0.0127	139.26380	139.26380	139.26380
.	-0.0254	117.36434	117.36434	117.36434
0.003175	-0.03175	105.97456	105.97456	105.97456

5. DISCUSSION AND CONCLUSION

Mathematical expressions for the magnetic field from a conical current sheet and a tightly-wound conical coil are found and compared. Also, mathematical expressions for the cylindrical current sheet are developed from the limiting case of the conical current sheet. The authors then compared the

mathematical expressions for the cylindrical current sheet to published results. The components of the magnetic field produced by a cylindrical current sheet yield exact mathematical expressions in terms of known special functions as is shown by Eqs. (64), (65), (68) and (69). However, for the conical current sheet, an infinite series solution in terms of Appell hypergeometric functions is found. Whether this series is summable in terms of some set of special functions has currently eluded the authors. Searching for a non-series solution to this problem may indeed be a worthwhile future research topic.

The main goal of this article is to develop a number of formulations which may be of interest to those who are either designing conical magnetic structures for the purpose of generating a magnetic field or for the purpose of optimization. Optimization methods can be expedited more readily when analytical expressions are available. It is not the intention of the authors to write a compendium of all possible forms for the solution of the magnetic field due to a conical current sheet, but to introduce a few expressions which may be used as a starting point for those who wish to design or analyze such structures.

There is a cost in computing values for special functions such as hypergeometric functions, elliptic integrals, Bessel functions, etc., as well as infinite series formulations, and this cost may be too great if one is interested in very fast and accurate computations. In general, what one tries to accomplish with any powerful numerical technique is speed and accuracy, and to limit the number of floating point operations. The authors have made no attempt to venture into the details of this important subject. What the authors have done is to numerically validate each mathematical expression introduced in this article. Although speed of computation is important, the authors' main interest was in the accuracy of the mathematical expressions. However, a number of integral expressions are developed for both conical current sheets and cylindrical current sheets and have proven to be numerically robust within the Mathematica [5] environment. For example, the reader will find that Eqs. (15), (16), (18), (19), (21), (22), (57), and (59) are quite robust when numerically evaluated by employing Mathematica's [5] intrinsic numerical integration algorithm. If speed and accuracy is the main purpose, then these equations perform well.

For the conical current sheet, application of Eqs. (26) and (31) should not be employed for purely numerical analysis. As with most purely analytical solutions, their real utility is often found not for their application in numerical analysis, but for their application in parametric studies such as optimization.

REFERENCES

1. Snow, C., "Magnetic fields of cylindrical coils and annular coils," *Natl. Bur. Stand., Appl. Math. Ser.*, Vol. 38, 1–29, Dec. 1953.
2. Snow, C., "Formula for the inductance of a helix made with wire of any section," *Sci. Pap. Bur. Stand.*, Vol. 21, No. 537, 431–519, Feb. 1926.
3. Jackson, J. D., *Classical Electrodynamics*, 3rd Edition, 180–181, John Wiley and Sons, New York, 1999.
4. Smythe, W. R., *Static and Dynamic Electricity*, 3rd Edition, 282–283, McGraw-Hill, New York, 1968.
5. Wolfram Research Inc., Mathematica, Version 12.1, Champaign, IL, 100 Trade Center Drive, 61820-7237, USA, 2020.
6. Hart, S., K. Hart, and J. P. Selvaggi, "Analytical expressions for the magnetic field from axially magnetized and conically shaped permanent magnets," *IEEE Trans. Magn.*, Vol. 56, No. 7, 1–9, Jul. 2020.
7. Flax, L. and E. Callaghan, "Magnetic field from a finite thin cone by use of Legendre polynomials," 1–41, NASA TN D-2400, Lewis Research Center, Cleveland, Ohio, USA, Aug. 1963.
8. Snow, C., "Formulas for computing capacitance and inductance," *National Bureau of Standards Circular*, Vol. 544, Sep. 1, 1954.
9. Snow, C., "Hypergeometric and legendre functions with applications to integral equations of potential theory," *Nat. Bur. Stand. Appl. Math. Ser.*, Vol. 19, 228–252, May 1, 1952.
10. Cohl, H. S. and J. E. Tohline, "A compact cylindrical Green's function expansion for the solution of potential problems," *The Astrophysical Journal*, Vol. 527, 86–101, Dec. 1999.

11. Cohl, H. S., A. R. P. Rau, J. E. Tohline, D. A. Browne, J. E. Cazes, and E. I. Barnes, "Useful alternative to the multipole expansion of $1/r$ potentials," *Phys. Rev. A*, Vol. 64, 052509-5, Oct. 2001.
12. Cohl, H. S., J. E. Tohline, and A. R. P. Rau, "Developments in determining the gravitational potential using toroidal functions," *Astron. Nachr.*, Vol. 321, 363–372, Nov. 2000.
13. Selvaggi, J. P., "Multipole analysis of circular cylindrical magnetic systems," Ph.D. dissertation, Rensselaer Polytech. Inst., Troy, NY, USA, 2005.
14. Selvaggi, J., S. Salon, O. Kwon, and M. V. K. Chari, "Calculating the external magnetic field from permanent magnets in permanent-magnet motors—an alternative method," *IEEE Trans.*, Vol. 40, No. 5, 3278–3285, Sep. 2004.
15. Selvaggi, J. P., S. Salon, and M. V. K. Chari, "An application of toroidal functions in electrostatics," *Am. J. Phys.*, Vol. 75, No. 8, 724–727, Apr. 2007.
16. Selvaggi, J. P., S. Salon, O. Kwon, and M. V. K. Chari, "Computation of the three-dimensional magnetic field from solid permanent-magnet bipolar cylinders employing toroidal harmonics," *IEEE Trans. Magn.*, Vol. 43, No. 10, 3833–3839, Oct. 2007.
17. Selvaggi, J. P., S. Salon, and M. V. K. Chari, "Computing the magnetic induction field due to a radially-magnetized finite cylindrical permanent magnet by employing toroidal harmonics," *PIERS Proceedings*, 244–251, Cambridge, USA, Jul. 5–8, 2010.
18. Selvaggi, J. P., S. Salon, and M. V. K. Chari, "Employing toroidal harmonics for computing the magnetic field from axially magnetized multipole cylinders," *IEEE Trans. Magn.*, Vol. 46, No. 10, 3715–3723, Oct. 2010.
19. Selvaggi, J. P., S. Salon, O. Kwon, and M. V. K. Chari, "Calculating the external magnetic field from permanent magnets in permanent-magnet motors — An alternative method," *IEEE Trans. Magn.*, Vol. 40, No. 5, 3278–3285, Sep. 2004.
20. Selvaggi, J. P., S. Salon, O. Kwon, and M. V. K. Chari, "Computation of the three-dimensional magnetic field from solid permanent-magnet bipolar cylinders employing toroidal harmonics," *IEEE Trans. Magn.*, Vol. 43, No. 10, 3833–3839, Oct. 2007.
21. Whittaker, E. T. and G. N. Watson, *A Course of Modern Analysis*, 4th Edition, 281–301, Cambridge at University Press, 1952.
22. Wang, Z. X. and D. R. Guo, *Special Functions*, 135–209, World Scientific, Singapore, 1989.
23. Hanson, M. T. and I. W. Puja, "The evaluation of certain infinite integrals involving products of Bessel functions: A Correlation of formula," *Quart. Appl. Math.*, Vol. 55, No. 3, 505–524, Sep. 1997.
24. Colavecchia, F. D., G. Gasaneo, and J. E. Miraglia, "Numerical evaluation of Appell's F_1 hypergeometric function," *Comp. Phys Comm.*, Vol. 138, 29–43, Mar. 2001.
25. Bailey, W. N., *Appell's Hypergeometric Functions of Two Variables, Ch. 9 in Generalised Hypergeometric Series*, 73–83 and 99–101, Cambridge University Press, Cambridge, England, 1935.
26. Byrd, P. F. and M. D. Friedman, *Handbook of Elliptic Integrals for Engineers and Physicists*, Springer-Verlag, Berlin Heidelberg GMBH, 1954.
27. Callaghan, E. E. and S. H. Maslen, "The magnetic field from a finite solenoid," 1–23, NASA TN D-465, Lewis Research Center, Cleveland, Ohio, USA, Oct. 1960.
28. Slater, L. J., *Generalized Hypergeometric Functions*, Cambridge Univ. Press, Cambridge, U.K., 1966.
29. Conway, J. T. "Exact solutions for the magnetic fields of axisymmetric solenoids and current distributions," *IEEE Trans. Magn.*, Vol. 37, No. 4, 2977–2988, Jul. 2001.
30. Brown, G. V. and L. Flax, "Superposition calculation of thick solenoid fields from semi-infinite solenoid tables," 1–23, NASA TN D-2494, Lewis Research Center, Cleveland, Ohio, USA, Sep. 1964.
31. Conway, J. T., "Exact solutions for the mutual inductance of circular coils and elliptic coils," *IEEE Trans. Magn.*, Vol. 48, No. 1, 81–94, Jan. 2012.
32. Conway, J. T., "Analytical solutions for the Newtonian gravitational field induced by matter within axisymmetric boundaries," *Mon. Not. R. Astron. Soc.*, Vol. 316, 540–554, Feb. 2000.
33. Conway, J. T., "Inductance calculations for circular coils of rectangular cross section and parallel axes using Bessel and Struve functions," *IEEE Trans. Magn.*, Vol. 46, No. 1, 75–81, Jan. 2010.

34. Conway, J. T., "Exact solutions for the mutual inductance of circular coils and elliptic coils," *IEEE Trans. Magn.*, Vol. 48, No. 1, 81–94, Jan. 2012.
35. Conway, J. T., "Inductance calculations for noncoaxial coils using Bessel functions," *IEEE Trans. Magn.*, Vol. 43, No. 3, 1023–1034, Mar. 2007.
36. Conway, J. T., "Noncoaxial inductance calculations without the vector potential for axisymmetric coils and planar coils," *IEEE Trans. Magn.*, Vol. 44, No. 4, 453–462, Apr. 2008.
37. Conway, J. T., "Non coaxial force and inductance calculations for bitter coils and coils with uniform radial current distributions," *2011 International Conference on Applied Superconductivity and Electromagnetic Devices*, 61–64, Sydney, NSW, 2011.
38. Babic, S., C. Akyel, J. Martinez, and B. Babic, "A new formula for calculating the magnetic force between two coaxial thick circular coils with rectangular cross-section," *Journal of Electromagnetic Waves and Applications*, Vol. 29, No. 9, 1181–1193, 2015.
39. Babic, S. and C. Akyel, "New formulas for mutual inductance and axial magnetic force between magnetically coupled coils: Thick circular coil of the rectangular cross-section-thin disk coil (pancake)," *IEEE Trans. Magn.*, Vol. 49, No. 2, 860–868, Feb. 2013.
40. Babic, S. I. and C. Akyel, "Calculating mutual inductance between circular coils with inclined axes in air," *IEEE Trans. Magn.*, Vol. 44, No. 7, 1743–1750, Jul. 2008.
41. Babic, S., F. Sirois, C. Akyel, G. Lemarquand, V. Lemarquand, and R. Ravaud, "New formulas for mutual inductance and axial magnetic force between a thin wall solenoid and a thick circular coil of rectangular cross-section," *IEEE Trans. Magn.*, Vol. 47, No. 8, 2034–2044, Aug. 2011.
42. Babic, S., F. Sirois, C. Akyel, G. Lemarquand, V. Lemarquand, and R. Ravaud, "Correction to "New formulas for mutual inductance and axial magnetic force between a thin wall solenoid and a thick circular coil of rectangular cross-section,"" *IEEE Trans. Magn.*, Vol. 48, No. 6, 2096–2096, Jun. 2012.
43. Ravaud, R., G. Lemarquand, S. Babic, V. Lemarquand, and C. Akyel, "Cylindrical magnets and coils: Fields, forces, and inductances," *IEEE Trans. Magn.*, Vol. 46, No. 9, 3585–3590, Sep. 2010.
44. Ravaud, R., G. Lemarquand, V. Lemarquand, and C. Depollier, "Analytical calculation of the magnetic field created by permanent-magnet rings," *IEEE Trans. Magn.*, Vol. 44, No. 8, 1982–1989, Aug. 2008.
45. Ravaud, R., G. Lemarquand, and V. Lemarquand, "Magnetic field created by tile permanent magnets," *IEEE Trans. Magn.*, Vol. 45, No. 7, 2920–2926, Jul. 2009.
46. Ravaud, R., G. Lemarquand, and V. Lemarquand, "Force and stiffness of passive magnetic bearings using permanent magnets. Part 1: Axial magnetization," *IEEE Trans. Magn.*, Vol. 45, No. 7, 2996–3002, Jul. 2009.
47. Ravaud, R., G. Lemarquand, and V. Lemarquand, "Force and stiffness of passive magnetic bearings using permanent magnets. Part 2: Radial magnetization," *IEEE Trans. Magn.*, Vol. 45, No. 9, 3334–3342, Sep. 2009.
48. Babic, S., C. Akyel, M. M. Gavrilovic, and K. Wu, "New closed-form expressions for calculating the magnetic field of thin conductors with azimuthal current direction," *4th International Conference on Telecommunications in Modern Satellite, Cable and Broadcasting Services. TELSIKS'99 (Cat. No.99EX365)*, Vol. 1, 44–47, Nis, Yugoslavia, 1999.
49. Stoll, J. C., P. L. Yohner, and J. C. Laurence, "Magnetic fields due to solid and hollow conical conductors," 1–131, NASA SP-3022, Lewis Research Center, Cleveland, Ohio, USA, Aug. 1965.